Molecular Biology of the Cell
Vol. 4, 233–246, February 1993

The Unconventional Myosin Encoded by the *myo*A Gene Plays a Role in *Dictyostelium* Motility

Margaret A. Titus,*†‡ Deborah Wessels,§ James A. Spudich,* and David Soll§

*Departments of Cell Biology and Developmental Biology, Stanford University School of Medicine, Stanford, California 94305; †Department of Cell Biology, Duke University Medical Center, Durham, North Carolina 27710; and §Department of Biology, University of Iowa, Iowa City, Iowa 52242

Submitted October 26, 1992; Accepted December 31, 1992

The *myo*A gene of *Dictyostelium* is a member of a gene family of unconventional myosins. The myosin Is share homologous head and basic domains, but the myoA gene product lacks the glycine-, proline-, alanine-rich and *src* homology 3 domains typical of several of the other myosin Is. A mutant strain of *Dictyostelium* lacking a functional *myo*A gene was produced by gene targeting, and the motility of this strain in buffer and a spatial gradient of the chemoattractant cyclic AMP was analyzed by computer-assisted methods. The *myo*A$^-$ cells have a normal elongate morphology in buffer but exhibit a decrease in the instantaneous velocity of cellular translocation, an increase in the frequency of lateral pseudopod formation, and an increase in turning. In a spatial gradient, in which the frequency of pseudopod formation is depressed, *myo*A$^-$ cells exhibit positive chemotaxis but still turn several times more frequently than control cells. These results demonstrate that the other members of the unconventional myosin family do not fully compensate for the loss of functional myoA gene product. Surprisingly, the phenotype of the *myo*A$^-$ strain closely resembles that of the *myo*B$^-$ strain, suggesting that both play a role in the frequency of pseudopod formation and turning during cellular translocation.

INTRODUCTION

Dictyostelium discoideum amoebas contain both the conventional filament-forming myosin and several nonfilamentous unconventional myosins (for reviews see Spudich, 1989; Pollard *et al.*, 1991). The conventional myosin is concentrated in the cortex of the posterior two-thirds of a translocating *Dictyostelium* amoeba (Fukui *et al.*, 1990), and either disruption, deletion (DeLozanne and Spudich, 1987; Manstein *et al.*, 1989), or inhibition of its expression via antisense constructs (Knecht and Loomis, 1987) of the single myosin heavy chain gene (*mhc*A) results in an amoeba defective in cytokinesis, cell shape, cell migration, cortical tension, intracellular particle movement, and the rapid response to 10^{-6} M cyclic AMP (cAMP) (reviewed in Spudich, 1989; Wessels and Soll, 1990).

There is a family of unconventional myosin genes in *Dictyostelium* (Titus *et al.*, 1989; Hammer, 1991), in contrast to the single gene that encodes the conventional myosin heavy chain (DeLozanne *et al.*, 1985). The best known of the unconventional myosins are the myosin Is, which are single-headed and remain monomeric under all in vitro conditions so far tested (for review see Korn and Hammer, 1988). Myosin Is have been purified both from *Acanthamoeba* (Pollard and Korn, 1973; Maruta *et al.*, 1979; Lynch *et al.*, 1989) and *Dictyostelium* (Cote *et al.*, 1985), and the *Acanthamoeba* myosin Is have been shown to be capable of generating movement in vitro (Albanesi *et al.*, 1985; Zot *et al.*, 1992). Although the head domains of the myosin Is are similar to each other as well as to the head regions of the conventional myosins, the tail regions differ significantly (Warrick and Spudich, 1987; Pollard *et al.*, 1991). There is a basic domain adjacent to the myosin I head that has been shown to bind to either positively charged phospholipid vesicles or NaOH-extracted plasma membranes (Adams and Pollard, 1989; Miyata *et al.*, 1989). The region of the *Acanthamoeba* myosin IC tail responsible for membrane binding has been mapped by in vitro studies and

‡ Corresponding author.

shown to be contained within amino acids 701 to 888 (Doberstein and Pollard, 1992). The C-terminus of the *Acanthamoeba* myosin Is comprise a second ATP-insensitive actin binding site (Lynch *et al.*, 1986; Doberstein and Pollard, 1992). The ATP-insensitive actin binding region is notable for the high content of glycine, proline, and alanine residues (GPA) and for the presence of an SH3 (*src* homology 3) (see Mayer *et al.*, 1988; Stahl *et al.*, 1988) region.

Higher eukaryotic and mammalian forms of myosin I have been identified. The chicken intestinal brush border myosin I resembles the protozoan myosin Is in that it is also monomeric and can generate movement in vitro (Collins and Borysenko, 1984; Conzelman and Mooseker, 1987; Mooseker and Coleman, 1989). This myosin I contains a calmodulin binding domain adjacent to the head, followed by a basic membrane binding domain (Carboni *et al.*, 1988; Coluccio and Bretscher, 1988; Hayden *et al.*, 1990). A mammalian myosin I that closely resembles the brush border myosin I recently has been isolated and characterized (Barylko *et al.*, 1992). It too has been localized at the leading edge of cells (Wagner *et al.*, 1992). Although much has been learned about the biochemical characteristics of these myosins, their precise in vivo role is poorly understood.

The capacity to disrupt genes in *Dictyostelium* by homologous recombination provides us with a means to assess individual unconventional myosin gene function in vivo. Five genes that encode unconventional myosins have so far been identified in *Dictyostelium* (Jung *et al.*, 1989; Titus *et al.*, 1989; Jung and Hammer, 1990). Sequence analysis of these five unconventional myosin genes reveals that they can be divided into two classes, based on differences in the tail structure. There is, therefore, a possibility of redundancy in function among these family members. The *myo*B[1], *myo*C, and *myo*D genes encode the *Dictyostelium* homologues of the well-described *Acanthamoeba* myosin Is (Hammer, 1991; Titus, unpublished data). The tail region of these *Dictyostelium* myosin Is contain the characteristic basic domain, followed by the GPA and SH3 regions (Jung *et al.*, 1989, 1990; Titus unpublished data). The *myo*A and *myo*E genes, however, encode what can be considered "short" myosin Is in that the heavy chain is smaller than that of the longer myosin Is (110 vs. 130 kDa). The myoA and myoE heavy chains are shorter due to the absence of the GPA and SH3 regions typical of the C-terminus of protozoan myosin Is (Titus *et al.*, 1989; Hammer, 1991). The differences in tail structure would suggest that these two types of unconventional myosin play distinct roles in cell behavior.

[1] The genes encoding the five unconventional myosins in *Dictyostelium* were originally referred to as myo1 (Jung *et al.*, 1989), *abm*A and *abm*C (Titus *et al.*, 1989), and DMID and DMIE (Urrutia *et al.*, 1990). Following the unifying nomenclature adopted by Kuspa *et al.* (1992), genes encoding the *Dictyostelium* unconventional myosins are now designated *myo*B, *myo*A, *myo*C, *myo*D, and *myo*E, respectively.

An analysis of myoB-deficient strains demonstrated that most basic aspects of cellular morphology, anteriorly biased pseudopod formation, F-actin localization, and responsiveness to the rapid addition of cAMP were normal in translocating cells (Wessels *et al.*, 1991). However, *myo*B$^-$ cells perfused with buffer lacking cAMP formed lateral pseudopodia roughly three times as frequently as normal cells, turned more frequently, and exhibited depressed average instantaneous velocities of cellular translocation when compared with *myo*B$^+$ control cells (Wessels *et al.*, 1991). These phenotypic abnormalities suggested that if there was a functional substitution for myoB by one or more of the other myosin I isoforms, it was at best partial. It was expected, therefore, that disruption of the *myo*A gene would lead to a behavioral phenotype distinct from that of *myo*B$^-$ cells. Here we have used gene targeting to construct cell lines that do not express functional myoA protein, and we have analyzed their behavior by computer-assisted motion analysis techniques (Soll, 1988; Soll *et al.*, 1987, 1988; Wessels *et al.*, 1989; Wessels and Soll, 1990). Our results suggest that the myoA and myoB gene products function in the same behavioral processes.

MATERIALS AND METHODS

Construction of Vectors

The transformation vector, pDTa13 (Figure 1), was constructed by first generating pDTa1R. This plasmid contained the 3.4-kilobase (kb) *Bgl* II fragment of the *myo*A gene (Titus *et al.*, 1989) ligated to *Bam*HI-cut pTZ-18R (Pharmacia Fine Chemicals, Piscataway, NJ) with the 5′ end of the *myo*A gene adjacent to the *Xba* I site of the pTZ-18R polylinker. Next, the plasmid pDTa4 was generated by digesting pDTa1R with both *Eco*RV and *Sma* I (in the polylinker adjacent to the 3′ end of the *myo*A gene) to remove the 2.4-kb 3′ fragment, adding dephosphorylated *Bgl* II linkers (New England Biolabs, Beverly, MA) and religating the shortened vector. The pDTa5R plasmid was then constructed by digesting pDTa4 with *Bgl* II and ligating the 2.1-kb neomycin drug resistance cartridge, liberated from pNeoMLS$^-$ (Manstein *et al.*, 1989) by a *Bam*HI and *Bgl* II digest to *Bgl* II-cut pDTa4. The pDTa5R plasmid contains the neomycin cartridge in the reverse orientation with respect to the *myo*A gene, i.e., with the terminator adjacent to the 5′ end of the truncated *myo*A gene (Figure 1, right). The pDTa1 plasmid (this plasmid is identical to pDTa1R except that the *Bgl* II fragment is present in the reverse orientation with respect to the polylinker, i.e., the 5′ end of the gene is adjacent to the *Sma* I site of the pTZ-18R polylinker) was digested with *Eco*RI and the internal 1.4- and 1.3-kb *Eco*RI fragments removed by gel purification. The remaining plasmid containing the 0.8-kb 3′ end of the *myo*A gene was religated and named pDTa6. The 0.8-kb *Eco*RI/*Pst* I fragment from pDTa6, containing the 3′ end of the *myo*A gene, which includes 0.2 kb of coding sequence and 0.6 kb of 3′ noncoding sequence, was liberated and treated with Klenow enzyme in the presence of excess deoxynucleotides to fill in the overhanging nucleotides generated from the restriction enzymes. This fragment was then ligated to pDTa5R that was cut with *Eco*RI and also treated with Klenow enzyme in the presence of nucleotides to fill in the overhanging nucleotides, resulting in the pDTa13 plasmid (Figure 1, top).

Maintenance of Stock Cultures

The axenic strain Ax-2 and both control and *myo*A$^-$ derivatives were grown according to methods previously described by Spudich (1982).

Stock cultures of all strains were stored at −70°C. For experiments assessing motility and chemotaxis, growth was initiated in 10-cm petri dishes containing 10 ml of the axenic growth medium HL-5 supplemented with 10 μg/ml G418. Cells were then transferred and maintained at 22°C in 15-cm petri dishes containing HL-5 medium plus G418.

Dictyostelium Transformation

The gene replacement fragment was liberated from pDTa13 by digestion with *Xba* I followed by phenol:chloroform extraction and ethanol precipitation. The total digest was then sequentially treated with calf intestinal alkaline phosphatase and Klenow enzyme (in the presence of excess deoxynucleotides). The treated digest was then extracted with phenol:chloroform and ethanol precipitated. *Dictyostelium* transformations were carried out using the modified calcium phosphate procedure described by Egelhoff *et al.* (1991). Discrete colonies were observed within 2 wk. Immediately after the appearance of discrete colonies, 30 individual colonies were randomly picked from the transformation plate and each transferred to an individual 100-mm petri dish containing 10 μg/ml G418 in HL-5 medium. New colonies were visible within 1 wk, and a single colony from each of the individual plates was picked and grown to confluence in a single well of a 24-well microtiter plate.

Screening for Homologous Integrants

DNA was prepared (Manstein *et al.*, 1989) from the individual clones in the 24-well plate to identify those clones where the pDTa13 vector was homologously integrated at the *myo*A locus. The clones were screened for the presence of homologous integrants using the polymerase chain reaction (PCR). The PCR primers corresponded to a region of the *myo*A gene upstream from the region of the predicted homologous integration event (nucleotides 206–226) (see Titus *et al.*, 1989), and the second was derived from the 3′ terminus of the Neo cassette, in the actin 15 terminator region (nucleotides 904–938 within the actin 15 sequence) (Knecht *et al.*, 1986). The sequences of the two oligonucleotides are shown below.

Primer 1 (1): 5′ GCTTACTGAAGTATCAGAATC 3′

Primer 2 (P2): 5′ CGATCAGCAATACCTGGGAACATAG 3′

The position of each of the primers is indicated in the diagram shown in Figure 1A. The successful integration of the pDTa13 gene replacement fragment at the 5′ end of the endogenous *myo*A gene predicts a 1.3-kb fragment after the PCR reaction. The PCR products were electrophoresed on a 0.7% agarose gel, transferred to nitrocellulose, and the blot probed with the 3.3-kb *Bgl* II fragment of the *myo*A gene (Titus *et al.*, 1989).

The nonhomologous transformants (*myo*A$^+$ strains nh4b and nh6b) are hereafter referred to as "controls" or "Ax2 controls", and homologous transformants (strains HTD1-12 and HTD1-19) are referred to as "mutants" or "*myo*A$^-$ amoebas."

Southern and Northern Blot Hybridization

DNA was prepared from cells according to Manstein *et al.* (1989) and total RNA purified by the method described by Nellen *et al.* (1987). Manipulation of DNA was carried out by standard methods (Sambrook *et al.*, 1989) and Southern and Northern blotting performed according to Howley *et al.* (1979). Blots were probed using random primed fragments labeled with ^{32}P-dATP. All of the enzymes used were obtained from Boehringer Mannheim Biochemicals (Indianapolis, IN).

Analysis of the Development of myoA$^-$ Cells

Control and mutant cells were treated identically. Cells were grown in 15-cm petri dishes containing HL-5 supplemented with 10 μg/ml G418 and harvested at a density of 6–7 × 10^7 cells/dish. Cells were gently scraped from growth plates, washed twice in BSS (buffered salt solution: 20 mM KCl, 0.24 mM $MgCl_2$, 40 mM phosphate buffer, pH 6.4, 0.34 mM streptomycin sulfate) (Soll, 1987), vortexed for 1 min, and plated onto 35-mm agar-coated petri dishes in 1.5 ml BSS at a density of 3 × 10^6 cells/dish (low density) or 4.5 × 10^6 cells/dish (high density) to initiate development. Cells developed to the tight aggregate stage submerged in buffer. The remaining liquid was removed from the dishes 24 h after plating so that development could proceed through the fruiting body stage. The number of fruiting bodies was then counted under the dissecting microscope 24 h after the removal of liquid from the dish. Two independent trials were performed in duplicate for each density for both control and mutant populations.

Computer-Assisted Analysis of Cellular Behavior

All the methods used have been described previously. Cells were developed on black pads before analysis as described in Soll (1987). Quantitation of cell shape, cell velocity, and pseudopod formation was performed as described in Varnum *et al.* (1985). The dynamic morphology and position of the cell centroid were determined using the Dynamic Morphology System (DMS) software (Soll, 1988; Soll *et al.*, 1987, 1988). Determinations of length, width, area, and roundness of a cell; instantaneous velocity of cellular translocation; and frequency of turning were made using established procedures (Soll, 1988; Soll *et al.*, 1987, 1988). The methods for quantitating pseudopod formation from difference pictures have been detailed in a previous publication (Wessels *et al.*, 1988). Computer-assisted analysis of cellular behavior and intracellular particle velocity before and after the addition of 10^{-6} M cAMP was carried out in a Dvorak-Stotler chamber as described (Wessels *et al.*, 1989, 1990; Wessels and Soll, 1990). Methods used to monitor behavior in a relatively stable gradient of cAMP were the same as those described in detail in previous reports (Varnum and Soll, 1984; Varnum-Finney *et al.*, 1987). Computer-assisted analysis of cellular behavior in a spatial gradient of cAMP was performed in a "Zigmond" chamber (Zigmond, 1977) with the sink containing buffer only and the trough filled with 10^{-7} M cAMP in BSS as described (Varnum and Soll, 1984). The chemotactic index was calculated from the centroid track as the directional distance (net distance toward the source) divided by the total distance traveled (McCutcheon, 1946; Varnum and Soll, 1984).

RESULTS

Generation of myoA$^-$ Cells

*myo*A$^-$ strains were prepared by gene targeting using the pDTa13 vector. A single transformation plate yielded in excess of 300 clones, 30 of which were randomly chosen for analysis. DNA was prepared from the transformants and PCR performed using the primers P1 and P2 to identify those clones where homologous integration of the pDTa13 gene replacement fragment had occurred at the *myo*A locus (Figure 1A, left). The expected 1.3-kb PCR product was obtained when the DNA from each of the 30 clones was analyzed (unpublished observation), indicating that the pDTa13 vector had integrated homologously at the 5′ end of the *myo*A gene in each clone. These clones were subjected to further study. The homologous integrants were named according to the system devised by Demerec *et al.* (1966) and are referred to as HTD1-1 through HTD1-30.

Several nonhomologous transformants were obtained by transformation of *Dictyostelium* with the circular pDTa5R plasmid (Figure 1A, right). Two of the transformants, nh6b and nh4b, contained the pDTa5R plas-

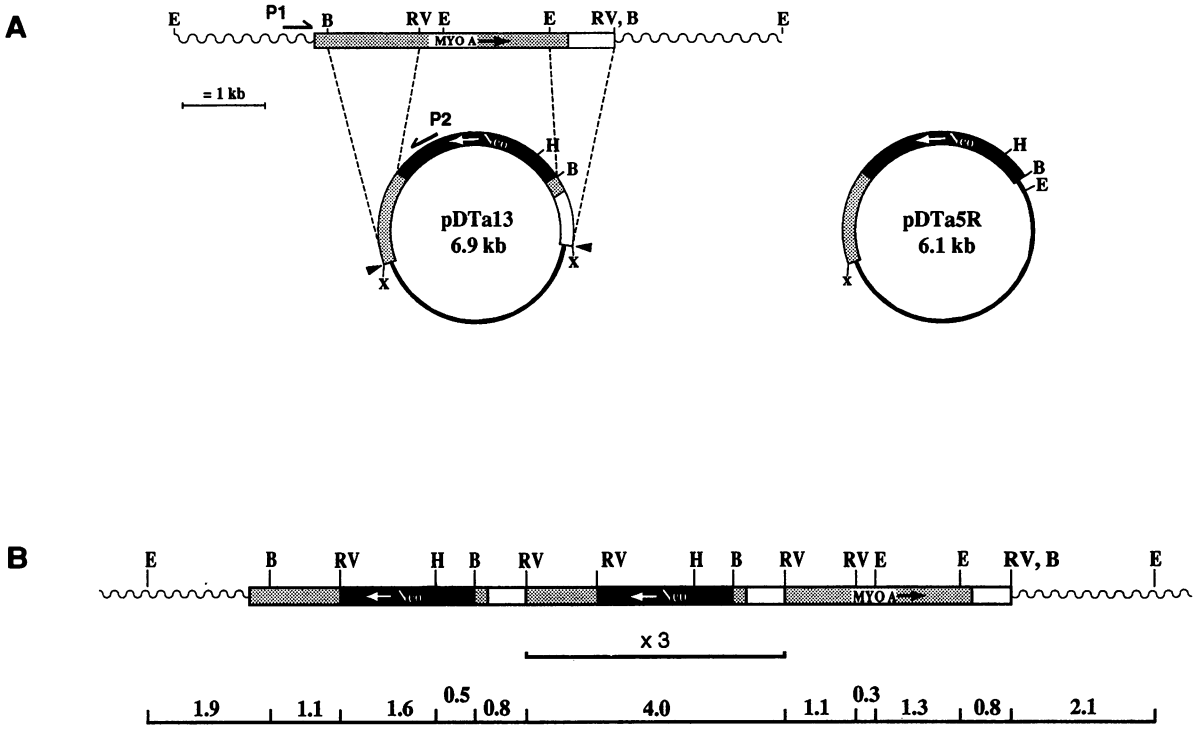

Figure 1. The *myo*A gene. (A) Construction of the gene replacement vector. Left, the *myo*A genomic locus is diagrammed with the pDTa13 plasmid shown below (not drawn to scale). The wavy lines indicate the extragenic region of the *myo*A gene, the grey box shows the coding region, and the unfilled box indicates the 3′ noncoding portion of the *myo*A gene. The direction of the *myo*A transcript is indicated by the arrow. The small black arrow labeled P1 indicates the position of the PCR primer P1. Indicated is the region of the *myo*A gene used to generate the pDTa13 vector (not to scale). The narrow line represents the *Escherichia coli* plasmid, the heavy black region the neomycin drug resistance cassette (Neo) with the white arrow representing the direction of transcription. The small arrows indicate the cleavage sites used to release the gene replacement fragment. The location of the PCR primer P2 is shown by the labeled arrow above the Neo cartridge. Right, a diagram of the nonhomologously integrating vector pDTa5R. This vector was used to generate the control nh4b and nh6b strains. The construct is similar to pDTa13 except for the absence a 3′ fragment of the *myo*A gene adjacent to the 5′ end of the Neo cartridge. (B) Deduced structure of the *myo*A locus in the HTD1 strains. The symbols are the same as described above, and the diagram is not drawn to scale. Shown directly below the diagram is a bracketed area marked with "× 3", indicating that this unit is repeated three times in the HTD1 strains; only one such repeat is shown for clarity. The numbers above the dark segmented line below the drawing of the locus indicate the distances, in kilobase, between the known restriction sites. Restriction sites are indicated by the letters B, *Bgl* II; E, *Eco*RI; RV, *Eco*RV; H, *Hind*III; and X, *Xba* I.

mid nonhomologously integrated into the genome and were used throughout this study as controls.

The integration event at the *myo*A locus in several randomly chosen independent transformants was determined by Southern analysis. An *Eco*RI/*Hind*III digest confirmed that the gene replacement fragment had inserted itself at the 5′ end of the *myo*A gene. The expected 4.3-kb *Eco*RI/*Hind*III band hybridized to probe A in the HTD1 strains (Figure 2A) instead of the 3.3-kb *Eco*RI band that would have been observed had no disruption of the *myo*A gene taking place (compare Figure 2, D with E). Surprisingly, the *myo*A gene was found not to have been eliminated in any of these cell lines based on the presence of a 2.6-kb *Eco*RV fragment that hybridized to an internal 1.3-kb *Eco*RI *myo*A fragment (probe B) that should have been lost (Figure 1B). This result suggested that the *myo*A gene was disrupted by insertion of the gene replacement vector at the 5′ end of the gene rather than having been eliminated by the gene replacement fragment, as expected. However, no detectable hybridization of a labeled pTZ-18R fragment to *Eco*RI digested HTD1 DNA was observed (unpublished observation), suggesting that a straightforward integration of an intact circular plasmid had not occurred. The size of the insertion event was determined by carrying out an *Eco*RI digestion of HTD1 DNA and hybridizing it to the 2.1-kb *Bam*HI/*Bgl* II fragment containing the Neo gene from pNeoMLS$^-$. A single fragment of 18.4 kb hybridized to probe C (Figure 2C), demonstrating that a multiple integration event had occurred solely at the *myo*A locus.

Based on the size of the fragment hybridizing to the Neo probe, the size of the gene replacement fragment (4.0 kb), and further detailed mapping studies (unpublished observation), it was surmised that four tandem copies of the gene replacement fragment were inserted in the *myo*A gene in each of the transformants, the arrangement of which is shown in Figure 1B. Such an

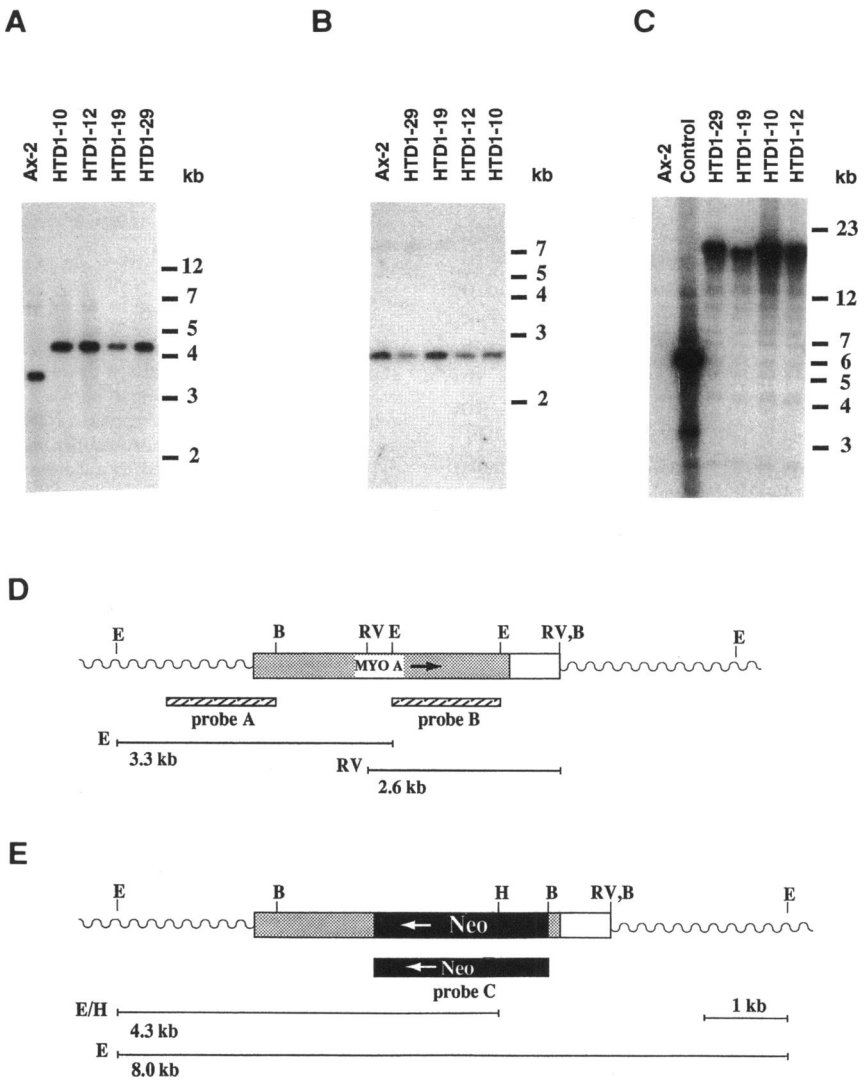

Figure 2. Southern analysis of the *myo*A gene disruption. (A) Analysis of the 5′ end of the *myo*A locus. Results of a Southern blot of DNA derived from four individual transformants (HTD1-10, -12, -19, -29) as compared with DNA from the wild-type Ax-2 strain (Ax-2). Genomic DNA prepared from wild-type and transformant strains (20 μg) was digested with *Eco*RI and *Hind*III, electrophoresed in an 0.8% agarose gel, transferred to nitrocellulose, and hybridized with a ^{32}P-labeled 1.4-kb *Eco*RI/*Bgl* II fragment of the 5′ noncoding region of the *myo*A gene (probe A, illustrated below in D). (B) Screen for an internal *myo*A fragment. DNA from the same strains as in A was digested with *Eco*RV and hybridized to probe B (shown in D). (C) Analysis of the size of inserted DNA at the *myo*A locus. DNA from wild-type and transformants was digested with *Eco*RI and hybridized to a 2.1-kb *Bam*HI/*Bgl* II fragment derived from pNEO-MLS$^-$ (Manstein *et al.*, 1989) that encompasses the Neo resistance cartridge (probe C, shown in E). The molecular weights of known DNA standards (kilobase) are shown on the right of each gel. (D) Structure of the *myo*A genomic locus. The symbols are the same as those shown in Figure 1. The two diagonally hatched boxes illustrate the positions of two of the probes used in the Southern analysis. Probe A corresponds to a 1.4-kb fragment derived from the 5′ end of the *myo*A gene (the probe was generated using *myo*A-specific primers in a PCR reaction) that was hybridized to the blot shown in A. Probe B corresponds to an internal 1.3-kb *Eco*RI fragment that was hybridized to the blot shown in B. The narrow lines indicate the expected size of the *Eco*RI (E) fragment detected by probe A in an *Eco*RI/*Hind*III double digest and the expected size of the *Eco*RV (RV) fragment detected by probe B in an *Eco*RV digest of wild-type DNA (bottom). (E) Predicted structure of the *myo*A locus after a straightforward gene replacement. The narrow lines below this diagram correspond to the fragments expected from either an *Eco*RI (E) or *Eco*RI/*Hind*III double digest (E/H) that would hybridize to probe A. No hybridization to probe B would be expected as this portion of the gene is predicted to be absent. The black box labeled Neo corresponds to probe C—the 2.1-kb neomycin drug resistance cassette—used in blot C. The scale, in kilobase, is shown at the bottom of E by the narrow line marked by 1 kb.

unusual insertion event is not unprecedented; unusual insertion events have been observed in some *mhc*A$^-$ strains (Manstein *et al.*, 1989).

The presence or absence of a full-length *myo*A RNA transcript in the HTD1 strains was determined by Northern analysis of several transformants. A 1.3-kb

Bgl II/*Eco*RI fragment derived from the 5′ coding region of the *myo*A gene (Titus *et al.*, 1989) was used as a probe. The *myo*A probe hybridized to the expected 3.8-kb transcript in both RNA from Ax2 cells (Figure 3A) and RNA from control (nh4b and nh6b) cells (unpublished observation). The HTD1 strains were found to express a *myo*A message of ~1.7 kb that hybridized to the probe (Figure 3A). The decreased size of the *myo*A message in the mutant strains is consistent with the predicted loss of 1.8 kb from the 3′ end of the coding region and absence of polyadenylation. The 1.7-kb *myo*A transcript observed in the HTD1 strains most likely does not code for functional *myo*A because the site of truncation, based on the integration of the pDTa13 construct, occurs midway between the ATP- and actin-binding regions of the myosin head (amino acid 344) (Titus *et al.*, 1989).

The level of expression of two other unconventional myosin genes, *myo*B and *myo*C (Jung *et al.*, 1989; Titus *et al.*, 1989), was examined in the *myo*A$^-$ strain HTD1-19 by Northern blotting. RNA was prepared from both wild-type Ax2 and *myo*A$^-$ cells that had been developed on starvation plates for both 3 and 6 h. The expression of *myo*B and *myo*C was unaltered in HTD1-19 (Figure 3, B and C).

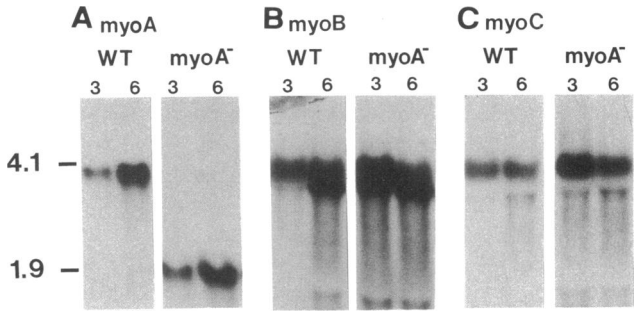

Figure 3. Expression of the *myoA*, *myoB*, and *myoC* genes in *myoA*$^-$ strain HTD1-19 after 3 and 6 h of development. Total cellular RNA was prepared from both wild-type Ax-2 (WT) and HTD1-19 (*myoA*$^-$) cells developed on starvation plates for both 3 and 6 h. A total of 12 μg of RNA was electrophoresed through a 1.25% agarose-formaldehyde gel and transferred to a Zetabind membrane. After prehybridization, the blots were hybridized in the same buffer (Church and Gilbert, 1984) with the following ^{32}P-labeled probes. (A) The 1.2-kb *Bgl* II/*Eco*RI fragment derived from the 5′ end of the *myoA* gene (see Figure 1, top); (B) an internal 2.3-kb *Bcl* I fragment derived from the *myoB* gene (Jung *et al.*, 1989); (C) a 1.9-kb *Bcl* I/*Hind*III fragment from the 5′ end of the *myoC* gene (Titus, unpublished data). The blots were washed twice with 0.5% bovine serum albumin, 5% sodium dodecyl sulfate, 80 mM sodium phosphate (pH 6.8), and 1 mM EDTA at 60°C for 15 min. The molecular weights of known RNA standards, in kilobase, are shown to the left of A.

Development of myoA$^-$ Cells

The developmental program is slightly delayed in the *myo*A$^-$ cells. Control amoebas exhibited the ripple stage (the onset of aggregation) (Soll, 1990) at 4 h at 22°C, and *myo*A$^-$ amoebas exhibited it at 4 h 40 min. The slight delay (14–15%) in the onset of aggregation was noted in five independent experiments for two different sets of control and *myo*A$^-$ amoebas. Both control and *myo*A$^-$ cells completed the morphogenetic program, forming fruiting bodies in both cases by 25 h. The *myo*A$^-$ cells, however, formed a reduced number of fruiting bodies when compared with the control strain. The total number of fruiting bodies formed when cells were plated at low density on agar-coated petri dishes was approximately half that of the control strain (146.8 ± 9.0 vs. 385.5 ± 15.1; mean ± SD). A similar effect was seen when cells were plated at a higher cell density (206.8 ± 25.8 vs. 435.2 ± 22.8).

Basic Morphology of myoA$^-$ Amoebas

The Ax2 control and *myo*A$^-$ amoebas (strains HTD1-12 and HTD1-19) were both capable of forming elongate cell morphologies (Figure 4), which has been demonstrated to be a characteristic of rapidly translocating aggregation-competent amoebas in strains Ax3 and Ax4 (Wessels *et al.*, 1989; Wessels and Soll, 1990). Both control amoebas (Figure 4, A–D) and *myo*A$^-$ amoebas (Figure 4, E–H) formed particulate-free anterior and lateral pseudopods and exhibited posterior ends with characteristic tail fibers. Control and *myo*A$^-$ cells could not be distinguished in qualitative comparisons (Figure 4). Quantitative analysis of length, width, area, and roundness of differential interference contrast (DIC) images demonstrated no significant differences between control and *myo*A$^-$ amoebas (unpublished observation). However, the DIC images of myoA$^-$ amoebas exhibited, on average, more lateral pseudopodia than control amoebas. Although 17% of 310 control cells exhibited three or more lateral pseudopodia, 63% of 355 *myo*A$^-$ cells did so. Lateral pseudopodia were identified as lateral protrusions free of particulate cytoplasm in this case (Figure 4).

Motility Characteristics of myoA$^-$ Amoebas are Altered in Buffer

The average instantaneous velocity computed from the path of the cell centroid was significantly different between control and *myo*A$^-$ cells translocating in buffer (Table 1). Control amoebas translocated at an average instantaneous velocity of 12.4 ± 4.6 μm/min, whereas *myo*A$^-$ amoebas translocated at 7.1 ± 2.9 μm/min. The difference was statistically significant at a $p < 0.005$ and similar to that observed between control Ax3 and *myo*B$^-$ amoebas (10.1 ± 2.8 and 5.2 ± 3.6 μm/min, respectively) (Wessels *et al.*, 1991).

Average positive (percentage of total cell area in expansion zones computed at 4-s intervals) and negative (percentage of total cell area in contraction zones computed at 4-s intervals) flow also differed between control

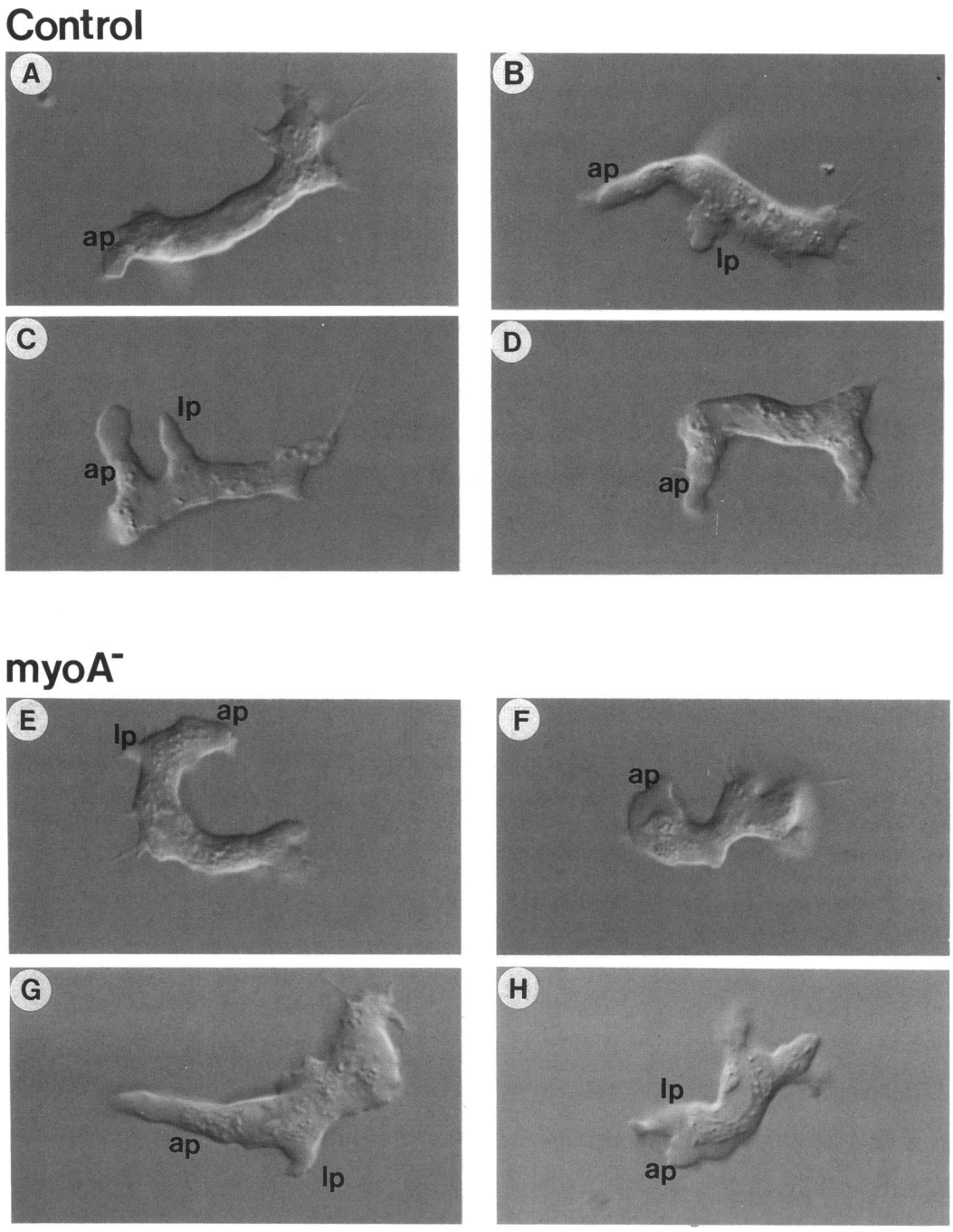

Figure 4. Differential interference contrast (DIC) micrographs of control (A–D) and *myo*A$^-$ (E–H) cells. Aggregation-competent amoebas were inoculated into the Dvorak-Stotler chamber and photographed with DIC optics using oil immersion of both the 63× Planapo objective (N.A. = 1.4) and the condensor (N.A. = 1.4). Note that both control and mutant amoebas achieve elongate morphologies and may simultaneously extend particulate free pseudopodia from both the ends of the cell (A, D, and E). Note also that the increased frequency of lateral pseudopod formation in *myo*A$^-$ amoebas gives rise to shapes such as those illustrated in H and G. lp indicates lateral pseudopodia and ap indicates anterior pseudopodia.

and *myo*A$^-$ cells, reinforcing the differences observed for instantaneous velocity. Average positive and negative flow were 14.6 ± 3.0%/4 s and 14.4 ± 3.0%/4 s, respectively, in control cells and 9.7 ± 3.9%/4 s and 9.7 ± 3.9%/4 s, respectively, in *myo*A$^-$ cells. The differences again were significant at $p < 0.001$.

Table 1. A comparison of motility and dynamic morphology parameters in the absence and presence of a spatial gradient of cAMP

	Instantaneous velocity (μm/min)	No. of pseudopodia per 5 min.	No. turns into pseudopodia per 5 min.	Initial pseudopodia area (%)	Maximum pseudopodia area (%)	Chemotactic index
In buffer (−cAMP)						
Control (n = 50)	12.4 ± 4.6	9.2 ± 6.0	2.3 ± 0.8	5.0 ± 3.6	19.0 ± 4.1	NA
*myo*A⁻ (n = 50)	7.1 ± 2.9	16.1 ± 6.7	4.3 ± 2.3	4.0 ± 2.1	10.0 ± 3.9	NA
p	<0.005	<0.001	<0.001	NS	<0.001	NA
In a spatial gradient of cAMP						
Control (n = 41)	11.1 ± 3.8	3.5 ± 1.6	0.7 ± 1.0	7.2 ± 1.0	17.5 ± 5.0	0.51
*myo*A⁻ (n = 41)	7.1 ± 3.4	4.5 ± 2.0	2.5 ± 1.4	5.3 ± 3.9	11.0 ± 6.4	0.28
p	<0.005	NS	<0.001	NS	<0.001	<0.01

Cells were inoculated at the loose aggregate stage into a Sykes-Moore chamber and perfused with buffer for analysis. After a 5-min acclimation period, cells were videorecorded for 5 min. For analysis in a spatial gradient, cells were inoculated in a gradient chamber, incubated for 5 min, and then recorded for 5 min. The videorecordings were automatically digitized for DMS analysis according to the procedures outlined in Methods. NA indicates not applicable, NS indicates not significant. Because of the negative and positive values for chemotactic index, a standard deviation was not calculated. An expansion zone was considered a pseudopod if it satisfied one of the following conditions: 1) it was elongated and comprised 3.5% or more of the total cell area at the time of appearance whether or not it continued to expand or 2) it was <3.5% of total cell area and continued to expand into an elongate extension (Wessels et al., 1988).

Pseudopod Dynamics and Turning of myoA⁻ Amoebas are Altered in Buffer

The increase in the number of particulate-free lateral pseudopods measured in the static DIC images of *myo*A⁻ cells in buffer was confirmed by quantitating the number of lateral expansion zones with pseudopod morphology formed per 5 min (Table 1; see footnote to define an expansion zone as a pseudopod). Control cells formed 9.2 ± 6.0 lateral pseudopodia per 5 min, whereas *myo*A⁻ cells formed 16.1 ± 6.7 per 5 min, close to twice the frequency of control cells. Interestingly, the increased frequency of pseudopod formation observed in the *myo*A⁻ strain is similar to that found in the *myo*B⁻ mutants (6 ± 3 per 5 min in control Ax3 cells vs. 16 ± 5 per 5 min in *myo*B⁻ cells) (Wessels *et al.*, 1991). The pseudopodia formed by *myo*A⁻ cells, on average, did not attain the maximum size of lateral pseudopodia formed by control cells in buffer (Table 1).

The increased frequency of pseudopod formation in *myo*A⁻ cells in buffer paralleled an increase in the number of turns into a pseudopod that a cell made during a 5-min period (Table 1). *myo*A⁻ cells turned, on average, 4.3 ± 2.3 times per 5 min, whereas control cells turned 2.3 ± 0.8 times per 5 min. The increase in the frequency of both pseudopod formation and turning had a pronounced effect on the translocation tracks of *myo*A⁻ cells, which is best visualized in stacked perimeter plots. Perimeter plots were generated by the DMS program for two representative control cells (Figure 5, A and B) and for two representative *myo*A⁻ cells (Figure 5, C and D) translocating in buffer. It is evident from a general comparison that there are far longer spans of persistent directional translocation in control plots than there are in *myo*A⁻ plots. The shorter spans of persistent translocation interspersed with frequent turns result in a more jerky path by the *myo*A⁻ cells (Figure 5, C and D). Although lateral pseudopods are usually retracted in the control perimeter plots (Figure 5, A and B), lateral pseudopods more frequently result in turns in the *myo*A⁻ perimeter plots (Figure 5, C and D). These differences were observed between the majority of 15 control and 15 *myo*A⁻ cells analyzed in this fashion.

Velocity and Turning of myoA⁻ Amoebas are Altered in a Spatial Chemotactic Gradient

*myo*A⁻ cells responded to a spatial gradient of cAMP by moving, on average, up the gradient. The average chemotactic index of 41 *myo*A⁻ cells was +0.28; 34 of the 41 *myo*A⁻ cells (83%) exhibited a positive chemotactic index. The average chemotactic index of 41 control cells was +0.51; 37 of the 41 control cells (90%) exhibited a positive chemotactic index. The instantaneous velocity of cellular translocation was also significantly lower in *myo*A⁻ cells in a spatial gradient (Table 1). The lower average chemotactic index of *myo*A⁻ cells may be the result of increased turning. It was previously demonstrated that a spatial gradient of cAMP depresses both the average frequency of lateral pseudopod formation and turning of strain Ax3 (Varnum-Finney *et al.*, 1987). The same was found to be true for both the Ax2 control and *myo*A⁻ cells in a spatial gradient (Table 1). Control cells decreased, on average, from 9.2 to 3.5 pseudopods per 5 min, and *myo*A⁻ cells decreased, on average, from 16.1 to 4.5 pseudopods per 5 min (Table 1). Therefore, the spatial gradient depressed the frequency of lateral pseudopod formation in *myo*A⁻ cells close to the min-

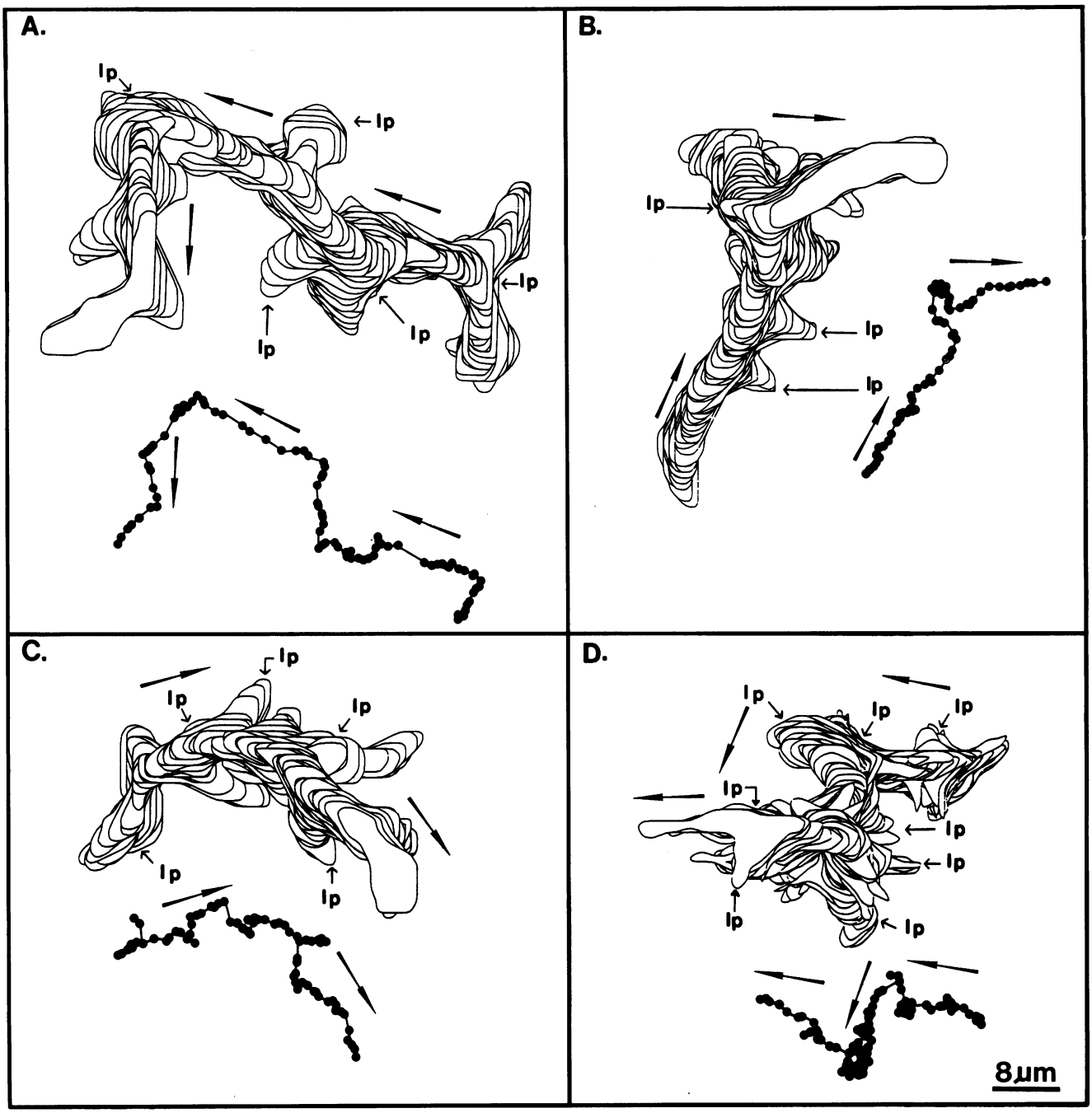

Figure 5. Perimeter plots and centroid plots of representative control (A and B) and *myo*A$^-$ (C and D) cells. Amoebas were removed from developmental filters at the onset of aggregation, inoculated into the Sykes-Moore perfusion chamber, and videorecorded during perfusion with buffer lacking chemoattractant. Cell perimeters were entered into the computer for analysis of motion and shape with DMS software as described in MATERIALS AND METHODS. Perimeters have been stacked at 4-s intervals. Note the increased frequency of lateral pseudopodia (lp) in the *myo*A$^-$ amoebas. Also note the periods of reduced translocation accompanied by complex shape changes in the mutants. The centroid plots are provided cell during the same period of analysis in the lower portion of each panel.

imum level of control cells. However, *myo*A$^-$ cells still turned more frequently than control cells. The *myo*A$^-$ cells turned into a lateral pseudopod 2.5 ± 1.4 times per 5 min, whereas control cells turned 0.7 ± 1.0 times per 5 min, almost a fourfold difference. In addition, the average maximum pseudopodia area of *myo*A$^-$ cells was significantly less than that of control cells in a spatial gradient (Table 1).

The difference in turning is evident in stacked perimeter plots. Perimeter plots were generated by the DMS program for two representative control cells (Figure 6, A and B) and for two representative *myo*A$^-$ cells (Figure 6, C and D) in a spatial gradient of cAMP. The gradient is increasing toward the top of the panel (noted by an arrow in the upper righthand corner) in each case. Control cells moved in a persistent fashion up the gradient. In the few cases where lateral pseudopods formed, they were retracted. This contrasts with the *myo*A$^-$ cells that formed lateral pseudopodia and turned into them more often (Figure 6, C and D). Therefore, although *myo*A$^-$ cells moved up the chemical gradient, they did so in a more jerky fashion, which is probably the basis for the lower average chemotactic index.

myoA$^-$ Cells Respond Normally to the Rapid Addition of 10^{-6} M cAMP

It was previously demonstrated that the rapid addition of 10^{-6} M cAMP to translocating *Dictyostelium* amoebas caused an abrupt cessation of cellular translocation and depression in intracellular particle velocity followed by

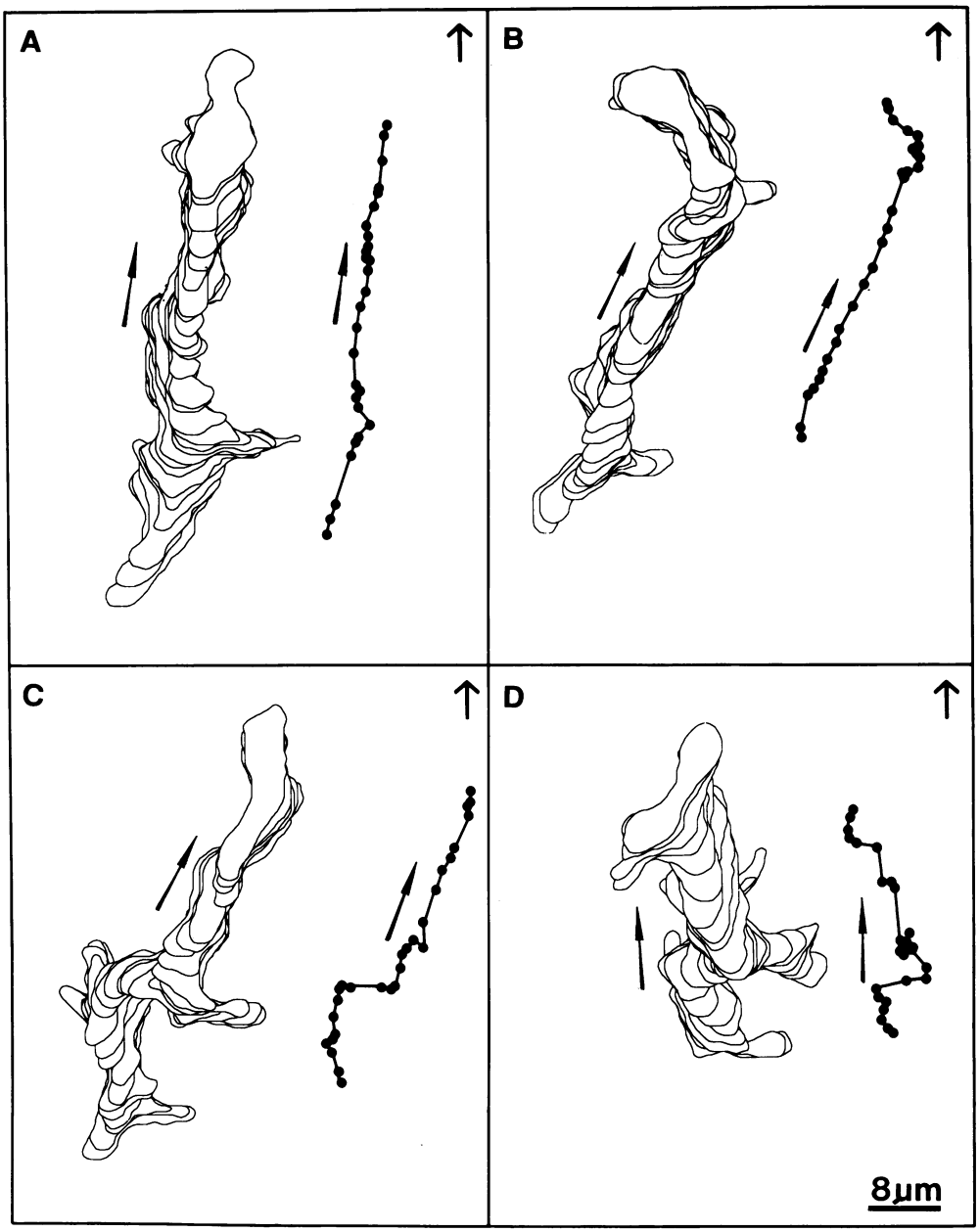

Figure 6. Perimeter and centroid plots of representative control (A and B) and representative *myo*A$^-$ (C and D) amoebas cells in spatial gradients of cAMP. Cell perimeters have been stacked at 4-s intervals. The source of cAMP is toward the top of the panel as indicated by the arrow in the upper right corner. The general direction of translocation is noted by tapered arrows. Note the increased frequency of lateral turns in the *myo*A$^-$ amoebas. The centroid plots are provided during the same period of analysis.

a partial rebound in both parameters (Wessels *et al.*, 1989, 1991). Although *myo*A$^-$ cells translocated at a slower rate than control cells, the rapid addition of 10^{-6} M cAMP resulted in the same rapid responses within seconds. This included an immediate decrease in instantaneous centroid velocity, an immediate decrease in the average velocity of intracellular particles, and an immediate freeze in cellular morphology. This was followed by a partial rebound, just as in the case of control cells. This response was observed qualitatively in 50 control nh4b, 50 control nh6b, 50 mutant HTD1-12, and 50 mutant HTD1-19 cells, and demonstrated quantitatively in 10 nh 4b and 10 HTD1-19 cells (unpublished observation).

DISCUSSION

Disruption of the *Dictyostelium myo*A gene leads to defects in cellular motility as determined by computer-assisted motion analysis (Soll, 1988; Soll *et al.*, 1987, 1988). The most surprising aspect of our findings is that the *myo*A$^-$ phenotype is similar to the *myo*B$^-$ phenotype (Table 2). Our results are unexpected because the myoA and myoB proteins differ in their C-termini. Both myosins have similar myosin head and basic domains, typical of myosin Is, yet they differ in that the myoB protein has a GPA/SH3 domain at the C-terminus that is lacking in the myoA protein (Jung *et al.*, 1989; Titus *et al.*, 1989). The tail domains of the various myosins are presumed to play an important role in localization and, by extension, intracellular function (Pollard *et al.*, 1991).

A quantitative analysis of the motility of the *myo*B$^-$ mutant was previously carried out in buffer alone (Wessels *et al.*, 1991), and we have performed identical experiments on the *myo*A$^-$ mutants and extended this analysis to include measurements on cells in a spatial gradient of cAMP. The *myo*A$^-$ and *myo*B$^-$ strains both have a normal elongate morphology yet have a lower average instantaneous velocity than control cells (Table 2). Detailed characterization of the dynamics of pseudopod formation in *myo*A$^-$ cells both in buffer and in a spatial gradient of cAMP reveals that the maximum size of the average lateral pseudopod, determined by expansion zones, is diminished. Pseudopods formed by *myo*B$^-$ cells in buffer are also, on average, smaller (Wessels *et al.*, 1991). More interestingly, both *myo*A$^-$ and *myo*B$^-$ cells form lateral pseudopodia more frequently than control cells translocating in buffer (Wessels *et al.*, 1991; this article). This increase is accompanied in both cases by an increase in the frequency of turning. It seems likely that the decrease in the instantaneous velocity of cellular translocation is, at least in part, a result of the increased frequencies of lateral pseudopod formation and turning.

Placing *myo*A$^-$ cells in a spatial gradient of attractant depresses the frequency of pseudopod extension to the basal level exhibited by control cells in a gradient (Table 1) (see Varnum-Finney *et al.*, 1987). Even though the frequency of pseudopod extension by *myo*A$^-$ cells in a spatial gradient is now that of control cells, the frequency at which *myo*A$^-$ cells turn into lateral pseudopods is still several times higher than that of control

Table 2. Summary of the behavioral phenotypes of cells lacking a myosin

Parameter	*mhc*A$^-$	*myo*B$^-$	*myo*A$^-$
Cell morphology	Round, nonpolar	Elongate, polar (WT)	Elongate, polar (WT)
Instantaneous cell centroid velocity	Decrease of 50%	Decrease of 50%	Decrease of 50%
Persistence of centroid translocation	No persistence	Decrease in persistence	Decrease in persistence
Frequency of lateral pseudopod extension in buffer	WT frequency	Increased (3- to 4-fold)	Increased (3- to 4-fold)
Direction of pseudopod extension in buffer	Random	Anterior bias (WT)	Anterior bias (WT)
Frequency of turning into lateral pseudopodia in buffer	Decreased	Increased (3-fold)	Increased (2-fold)
Effect of rapid addition of cAMP on instantaneous cell centroid velocity	No effect	Inhibition (WT kinetics)	Inhibition (WT kinetics)
Effect of rapid addition of cAMP on instantaneous particle velocity	None	Inhibition (WT kinetics)	Inhibition (WT kinetics)
Chemotaxis	Slightly positive	NA	Positive, but lower than WT
Aggregation	Delayed	Slight delay	Slight delay
Terminal development	Blocked at ripple stage (onset of aggregation)	Fruiting body (WT)	Fruiting body (WT)[a]

Several salient motile behaviors of *Dictyostelium* are listed. The behaviors of the mutant cell lines are compared with those of wild-type. Where the behavior of the mutant cells is indistinguishable from that of wild-type *Dictyostelium*, the comment is followed by WT. *mhc*A$^-$, cells devoid of the conventional myosin (data compiled from Wessels et al., 1988; Wessels & Soll, 1990); *myo*B$^-$, cells devoid of the myoB unconventional myosin (Jung & Hammer, 1990; Wessels et al., 1991); *myo*A$^-$, cells devoid of the *myo*A unconventional myosin (this article). NA, not assessed.

[a] It is demonstrated in this report that a carpet of *myo*A$^-$ cells forms fewer fruiting bodies than a carpet of wild-type cells.

cells (Table 1). Thus, even though roughly the same proportion of *myo*A$^-$ and control cells in a gradient exhibit a positive chemotactic index, the average chemotactic index of *myo*A$^-$ cells is lower than that of control cells (Table 1) because of the zig-zagging translocation pattern caused by the increased frequency of turning. Both the slower instantaneous velocity of cellular translocation and lower chemotactic index exhibited by the *myo*A$^-$ cells may contribute to a delay of aggregation in vivo (Jung and Hammer, 1990; this article).

These results raise questions regarding the functional significance of the differences in the tail regions of the two classes of unconventional myosins in *Dictyostelium*. The tails of the unconventional myosins are assumed to be responsible for determining the intracellular localization of these motor proteins and, by extension, their intracellular role (Pollard *et al.*, 1991). The *Acanthamoeba* myosins IA and IB have been shown to bind to the plasma membrane primarily via a direct interaction with the membrane and not through association with membrane-bound actin (Adams and Pollard, 1989; Miyata *et al.*, 1989). The region responsible for this interaction recently has been mapped in vitro and found to be contained within the basic domain adjacent to the myosin head region (Doberstein and Pollard, 1992). The myoA and myoB proteins both have a tail region that is highly homologous to the *Acanthamoeba* myosin I membrane binding domain (Jung *et al.*, 1989; Titus *et al.*, 1989). The similar phenotype of the *myo*A$^-$ and *myo*B$^-$ strains suggests that this region may dictate a common role in the frequency of pseudopod formation and cell turning.

Our results differ from those recently found for the *Drosophila nina*C myosin, where it is likely that differences in the C-termini of the *nina*C myosin tails determine their respective intracellular functions. The two *nina*C myosins are generated by alternate 3′ processing signals and they differ only at their C-termini (Montell and Rubin, 1988). The two *nina*C myosins are localized differentially. The longer form, p174, is specifically located in the rhabdomere and the shorter form (p132) is located in the extrarhabdomeral cytoplasm (Porter *et al.*, 1992). Elimination of the p174 myosin results in retinal degeneration and a phototransduction phenotype, whereas elimination of p132 results in no identifiable phenotype (Porter *et al.*, 1992).

The existence of at least five unconventional myosin genes in the haploid genome of *Dictyostelium* (Jung *et al.*, 1989, 1990; Titus *et al.*, 1989; Jung and Hammer, 1990) has led to the expectation that disruption of one of these genes might be compensated for by expression of one or more of the remaining four genes, resulting in no distinguishable phenotype. This is not the case. Analysis of the behavior of a *myo*B$^-$ strain (Jung and Hammer, 1990; Wessels *et al.*, 1991) and the results presented here show that if there is functional overlap between the various unconventional myosins it is, at best, partial. Analysis of the phenotypes of mutant strains suggests that both the myoA and myoB proteins play a role in both the suppression of improper lateral pseudopod formation and unnecessary turning. The role that the myoA and myoB unconventional myosins play in pseudopod morphogenesis is consistent with the localization of at least one of them, the myoB protein, in the distal edges of expanding pseudopodia (Fukui *et al.*, 1989).

Comparison of the phenotype of the *myo*A$^-$ cells with that of the *myo*B$^-$ and conventional myosin null cells illustrates how these different myosins play different roles in *Dictyostelium* motility. Disruption of the conventional myosin heavy chain gene (DeLozanne and Spudich, 1987; Manstein *et al.*, 1989) or selective inhibition of its expression by antisense constructs (Knecht and Loomis, 1989) results in severe defects in cell motility (Wessels *et al.*, 1988; Wessels and Soll, 1990; Fukui *et al.*, 1990). The conventional myosin is absolutely required for normal cytokinesis, capping, and cortical tension, roles consistent with its localization within the cell (reviewed in Spudich, 1989). The conventional myosin null cells are incapable of developing normal cell polarity, exhibit little persistent cellular translocation, exhibit little bias in the direction of pseudopod expansion, are unresponsive to the rapid addition of cAMP, and exhibit depression in the velocity and a loss of polarity of intracellular particle movement (Wessels and Soll, 1990). These defects in cellular motility may be due to an overall loss of cortical tension required for proper maintenance of cell shape and morphogenesis (Pasternak *et al.*, 1989) rather than to a direct role of the conventional myosin in cellular translocation. These alterations in behavior contrast with the common motility defects observed in the *myo*A$^-$ and *myo*B$^-$ strains that appear to be restricted to the frequency of pseudopod formation and turning (Table 2).

The phenotype of the *myo*A$^-$ and *myo*B$^-$ strains suggests that these myosins do not play essential roles in motility but rather are involved in fine tuning the dynamics of pseudopod extension. Either of these myosin Is could be required for stabilizing the actin filament network rather than playing a direct role in pseudopod extension. Although the gross actin distribution within the *myo*B$^-$ cells does not appear to be significantly altered (Wessels *et al.*, 1991), this does not rule out changes in the distribution of actin that remain undetected by fluorescence microscopy. A failure to properly cross-link the actin network could result in an increase in the frequency of formation of smaller pseudopods. The net effects of these changes would be a decrease in the persistence of cellular translocation. Given that a mutation in either the *myo*A or *myo*B gene results in the same aberrant phenotype, it will be informative to characterize the behavioral phenotype of cells with simultaneous mutations in both genes.

ACKNOWLEDGMENTS

We thank the members of the Spudich lab for ongoing discussions and advice. Particular thanks go to Drs. Hans Warrick and Janet Smith for invaluable comments and suggestions throughout this project as well as for their thorough reading of the manuscript. Also, thanks are due to Drs. Linda Silveira and Holly Goodson for many helpful suggestions that improved the manuscript. M.A.T. thanks Dr. Maureen Pupillo for helpful discussions and for sharing the PCR technique for detecting homologous transformants, Dr. Angelika Noegel for providing the Ax-2 strain, and Kris Novak for assistance with the RNA samples. We are grateful to Anand Chandrasekhar for carrying out the Northern blot analysis shown in Figure 3. The initial portions of this work were supported by an NIH postdoctoral fellowship (GM-12000) and subsequently by an NIH grant (GM-46486) to M.A.T. This work was also funded by NIH grants GM-40509 to J.A.S. and HD-18577 to D.R.S.

REFERENCES

Adams, R.J., and Pollard, T.D. (1989). Binding of myosin I to membrane lipids. Nature *340*, 565–568.

Albanesi, J.P., Fujisaki, H., Hammer, J.A., III, Korn, E.D., Jones, R., and Sheetz, M.P. (1985). Monomeric *Acanthamoeba* myosins I support movement in vitro. J. Biol. Chem. *260*, 8649–8652.

Barylko, B., Wagner, M.C., Reizes, O., and Albanesi, J.P. (1992). Purification and characterization of a mammalian myosin I. Proc. Natl. Acad. Sci. USA *89*, 490–494.

Carboni, J.M., Conzelman, K.A., Adams, R.A., Kaiser, D.A., Pollard, T.D., and Mooseker, M.S. (1988). Structural and immunological characterization of the myosin-like 110-kD-calmodulin complex: evidence for discrete myosin head and calmodulin-binding domains. J. Cell Biol. *107*, 1749–1757.

Church, G., and Gilbert, W. (1984). Genomic sequencing. Proc. Natl. Acad. Sci. USA *81*, 1991–1995.

Collins, J.H., and Borysenko, C.W. (1984). The 110,000-dalton actin- and calmodulin-binding protein from intestinal brush border is a myosin-like ATPase. J. Biol. Chem. *259*, 14128–14135.

Coluccio, L.M., and Bretscher, A. (1989). Mapping of the mirovillar 110K-calmodulin complex-calmodulin-associated or calmodulin-free fragment of 110KD polypeptide bind F-actin and retain ATPase activity. J. Cell Biol. *106*, 367–373.

Conzelman, K.A., and Mooseker, M.S. (1987). The 110-kD protein-calmodulin complex of the intestinal microvillus is an actin-activated MgATPase. J. Cell Biol. *105*, 313–324.

Cote, G.P., Albanesi, J.P., Ueno, T., Hammer, J.A., III, and Korn, E.D. (1985). Purification from *Dictyostelium discoideum* of a low-molecular weight myosin that resembles myosin I from *Acanthamoeba castellanii*. J. Biol. Chem. *260*, 4543–4546.

DeLozanne, A., Lewis, M., Spudich, J.A., and Leinwand, L.A. (1985). Cloning and characterization of a nonmuscle myosin heavy chain. Proc. Natl. Acad. Sci. USA *82*, 6807–6810.

DeLozanne, A., and Spudich, J.A. (1987). Disruption of the *Dictyostelium* myosin heavy chain gene by homologous recombination. Science *236*, 1086–1091.

Demerec, M., Adelberg, E., Clark, A., and Hartman, P. (1966). A proposal for a uniform nomenclature in bacterial genetics. Genetics *54*, 61–67.

Doberstein, S.K., and Pollard, T.D. (1992). Localization and specificity of the phospholipid and actin binding sites on the tail of *Acanthamoeba* myosin IC. J. Cell Biol. *117*, 1241–1249.

Egelhoff, T.T., Titus, M.A., Manstein, D.J., Ruppel, K.M., and Spudich, J.A. (1991). Molecular genetic tools for study of the cytoskeleton in *Dictyostelium*. Methods Enzymol. *196*, 319–334.

Fukui, Y., DeLozanne, A., and Spudich, J.A. (1990). Structure and function of the cytoskeleton of a *Dictyostelium* myosin-defective mutant. J. Cell Biol. *110*, 367–378.

Fukui, Y., Lynch, T.J., Brzeska, H., and Korn, E.D. (1989). Myosin I is located at the leading edges of locomoting *Dictyostelium* amoebas. Nature *341*, 328–331.

Hammer, J.A., III (1991). Novel myosins. Trends Cell Biol. *1*, 50–56.

Hayden, S.M., Wolenski, J.S., and Mooseker, M.S. (1990). Binding of brush border myosin I to phospholipid vesicles. J. Cell Biol. *111*, 443–451.

Howley, P.M., Israel, M.A., Law, M.F., and Martin, M.A. (1979). A rapid method for detecting and mapping homology between heterologous DNAs. Evaluation of polyomavirus genomes. J. Biol. Chem. *254*, 4876–4883.

Jung, G., and Hammer, J.A., III (1990). Generation and characterization of *Dictyostelium* cells deficient in a myosin I heavy chain isoform. J. Cell Biol. *110*, 1955–1964.

Jung, G., Saxe, C.L., III, Kimmel, A.R., and Hammer, J.A., III (1989). *Dictyostelium discoideum* contains a gene encoding a myosin I heavy chain isoform. Proc. Natl. Acad. Sci. USA *86*, 6186–6190.

Jung, G., Urrutia, R., and Hammer, J.A., III (1990). Myosins IB and ID appear to be the only members of one subgroup of *Dictyostelium* myosin I (MI) isoforms. J. Cell Biol. *111*, 168a.

Knecht, D.A., Cohen, S.M., Loomis, W.F., and Lodish, H.F. (1986). Developmental regulation of *Dictyostelium discoideum* actin gene fusions carried on low-copy and high-copy transformation vectors. Mol. Cell. Biol. *6*, 3973–3983.

Knecht, D.A., and Loomis, W.F. (1987). Antisense RNA inactivation of myosin heavy chain gene expression in *Dictyostelium discoideum*. Science *236*, 1081–1086.

Korn, E.D., and Hammer, J.A., III (1988). Myosins of nonmuscle cells. Annu. Rev. Biophys. Biophys. Chem. *17*, 23–45.

Kuspa, A., Maghakian, D., Bergesch, P., and Loomis, W.F. (1992). Physical mapping of genes to specific chromosomes in *Dictyostelium discoideum*. Genomics *13*, 49–61.

Lynch, T.J., Albanesi, J.P., Korn, E.D., Robinson, E.A., Bowers, B., and Fujisaki, H. (1986). ATPase activities and actin binding properties of subfragments of *Acanthamoeba* myosin IA. J. Biol. Chem. *261*, 17156–17162.

Lynch, T.J., Brzeska, H., Miyata, H., and Korn, E.D. (1989). Purification and characterization of a third isoform of myosin I from *Acanthamoeba castellanii*. J. Biol. Chem. *264*, 19333–19339.

Manstein, D.J., Titus, M.A., DeLozanne, A., and Spudich, J.A. (1989). Gene replacement in *Dictyostelium:* generation of myosin null mutants. EMBO J. *8*, 923–932.

Maruta, H., Gadasi, H., Collins, J.H., and Korn, E.D. (1979). Multiple forms of *Acanthamoeba* myosin I. J. Biol. Chem. *254*, 3624–3630.

Mayer, B.J., Hamaguchi, M., and Hanafusa, H. (1988). A novel viral oncogene with structural similarity to phospholipase-C. Nature *332*, 272–275.

McCutcheon, M. (1946). Chemotaxis in leukocytes. Physiol. Rev. *26*, 319–336.

Miyata, H., Bowers, B., and Korn, E.D. (1989). Plasma membrane association of *Acanthamoeba* myosin I. J. Cell Biol. *109*, 1519–1528.

Montell, C., and Rubin, G.M. (1988). The *Drosophila ninaC* locus encodes two photoreceptor cell specific proteins with domains homologous to protein kinases and the myosin heavy chain head. Cell *52*, 757–772.

Mooseker, M.S., and Coleman, T.R. (1989). The 110-kD protein-calmodulin complex of the intestinal microvillus (brush border myosin I) is a mechanoenzyme. J. Cell Biol. *108*, 2935–2400.

Nellen, W., Datta, S., Reymond, C., Sivertsen, A., Mann, S., Crowley, T., and Firtel, R.A. (1987). Molecular biology in *Dictyostelium:* tools and applications. *Dictyostelium discoideum:* molecular approaches to cell biology. Methods Cell Biol. *28*, 67–100.

Pasternak, C., Spudich, J.A., and Elson, E.L. (1989). Capping of surface receptors and concomitant cortical tension are generated by conventional myosin. Nature *341*, 541–549.

Pollard, T.D., Doberstein, S.K., and Zot, H.G. (1991). Myosin I. Annu. Rev. Physiol. *53*, 653–681.

Pollard, T.D., and Korn, E.D. (1973). *Acanthamoeba* myosin. I. Isolation from *Acanthamoeba castellanii* of an enzyme similar to muscle myosin. J. Biol. Chem. *248*, 4682–4690.

Porter, J.A., Hicks, J.L., Williams, D.S., and Montell, C. (1992). Differential localizations of and requirements for the two *Drosophila ninaC* kinase/myosins in photoreceptor cells. J. Cell Biol. *116*, 683–693.

Sambrook, J., Fritsch, E.F., and Maniatis, T. (1989). *Molecular Cloning: A Laboratory Manual.* 2nd ed. Cold Spring Harbor, NY: Cold Spring Harbor Laboratory.

Soll, D.R. (1987). Methods for manipulating and investigating developmental timing in *Dictyostelium discoideum. Dictyostelium discoideum:* molecular approaches to cell biology. Methods Cell Biol. *28*, 413–441.

Soll, D.R. (1988). "DMS," a computer-assisted system for quantitating motility, the dynamics of cytoplasmic flow and pseudopod formation: its application to *Dictyostelium* chemotaxis. Cell Motil. Cytoskeleton (Suppl.) *10*, 91–106.

Soll, D.R. (1990). Regulation of timing in *Dictyostelium* morphogenesis and other developing systems. In: Molecular Approaches to Supramolecular Phenomena. ed. S. Roth, Philadelphia, PA: University of Pennsylvania Press, 1–82.

Soll, D.R., Voss, E., Varnum-Finney, B., and Wessels, D. (1988). The "Dynamic Morphology System": a method for quantitating changes in shape, pseudopod formation and motion in normal and mutant amoebas of *Dictyostelium discoideum.* J. Cell. Biochem. *37*, 177–192.

Soll, D.R., Voss, E., and Wessels, D. (1987). Development and application of the "Dynamic Morphology System" for the analysis of moving amebae. Proc. Soc. Photo-op. Instr. Eng. *832*, 821–830.

Spudich, J.A. (1982). *Dictyostelium discoideum:* methods and perspectives for study of cell motility. Methods Cell Biol. *25* (part B), 359–364.

Spudich, J.A. (1989). In pursuit of myosin function. Cell Regul. *1*, 1–11.

Stahl, M.L., Ferenz, C.R., Kelleher, K.L., Kriz, R.W., and Knopf, J.L. (1988). Sequence similarity of phospholipase-C with a non-catalytic region of *src.* Nature *332*, 269–272.

Titus, M.A., Warrick, H.M., and Spudich, J.A. (1989). Multiple actin-based motor genes in *Dictyostelium.* Cell Regul. *1*, 55–63.

Urrutia, R., Jung, G., and Hammer, J.A., III (1990). Cloning and characterization of the *Dictyostelium* myosin IE gene. J. Cell Biol. *111*, 168a.

Varnum, B., Edwards, K.B., and Soll, D.R. (1985). *Dictyostelium* amebae alter motility differently in response to increasing versus decreasing temporal gradients of cAMP. J. Cell Biol. *101*, 1–5.

Varnum, B., and Soll, D.R. (1984). Effects of cAMP on single cell motility in *Dictyostelium.* J. Cell Biol. *99*, 1151–1155.

Varnum-Finney, B., Voss, E., and Soll, D.R. (1987). Frequency and orientation of pseudopod formation of *Dictyostelium discoideum* amebae chemotaxing in a spatial gradient: further evidence for a temporal mechanism. Cell Motil. Cytoskeleton *8*, 18–26.

Wagner, M.C., Barylko, B., and Albanesi, J.P. (1992). Tissue distribution and subcellular localization of mammalian myosin I. J. Cell Biol. *119*, 163–170.

Warrick, H.M., and Spudich, J.A. (1987). Myosin structure and function in cell motility. Annu. Rev. Cell Biol. *3*, 379–421.

Wessels, D., Murray, J., Jung, G., Hammer, J.A., III, and Soll, D.R. (1991). Myosin IB null mutants of *Dictyostelium* exhibit abnormalities in movement. Cell Motil. Cytoskeleton *20*, 301–315.

Wessels, D., Schroeder, N.A., Voss, E., Hall, A.L., Condeelis, J., and Soll, D.R. (1989). cAMP-mediated inhibition of intracellular particle movement and actin reorganization in *Dictyostelium.* J. Cell Biol. *109*, 2841–2851.

Wessels, D., and Soll, D.R. (1990). Myosin II heavy chain null mutant of *Dictyostelium* exhibits defective intracellular particle movement. J. Cell Biol. *111*, 1137–1148.

Wessels, D., Soll, D.R., Knecht, D.A., Loomis, W.F., DeLozanne, A., and Spudich, J.A. (1988). Cell motility and chemotaxis in *Dictyostelium* amebae lacking myosin heavy chain. Dev. Biol. *128*, 164–177.

Zigmond, S.H. (1977). The ability of polymorphonuclear leukocytes to orient in gradients of chemotactic factors. J. Cell Biol. *75*, 606–616.

Zot, H.G., Doberstein, S.K., and Pollard, T.D. (1992). Myosin-I moves actin filaments on a phospholipid substrate: implications for membrane targeting. J. Cell Biol. *116*, 367–376.